

# Annual intensification of the Somali jet in a quasi-equilibrium framework: Observational composites

William R. Boos<sup>a\*</sup> and Kerry A. Emanuel<sup>b</sup>

<sup>a</sup>*Dept. of Earth and Planetary Sciences, Harvard University, Cambridge, Mass, USA*

<sup>b</sup>*Program in Atmospheres, Oceans, and Climate, Massachusetts Institute of Technology, Cambridge, Mass, USA*

**ABSTRACT:** The annual intensification of the Somali jet, which accompanies the onset of the Indian summer monsoon, is rapid compared to the evolution of the seasonal insolation forcing. Using observationally-based data sets, the dynamic and thermodynamic changes accompanying the onset of this jet are presented. The abrupt component of jet onset is shown to occur over ocean about 1000 km east of the East African highlands, and is accompanied by increases in both deep convection and baroclinic flow over the off-equatorial Arabian Sea. These abrupt changes are well separated from the core of the cross-equatorial jet, which is located over land adjacent to the East African highlands.

The onset of the Somali jet and the associated monsoon are then examined in a convective quasi-equilibrium framework. Such a framework is consistent with the mean summer state, in that peak free-tropospheric temperatures are nearly collocated with peak subcloud layer entropies over the northern Bay of Bengal and adjacent coastal regions. Jet onset is accompanied by a large ( $O\{100 \text{ W m}^{-2}\}$ ) increase in surface enthalpy flux over the Arabian Sea that is nearly collocated with, and linearly related to, the concurrent increase in deep tropospheric ascent. At the same time, the highest subcloud entropies shift inland slightly from the Bay of Bengal, and the region of warmest free-tropospheric temperatures expands poleward. The consistency of all of these changes with a wind–evaporation feedback and several other hypothesized mechanisms of abrupt monsoon onset is discussed. Copyright © 2009 Royal Meteorological Society

KEY WORDS monsoon onset; Hadley circulation; Findlater jet

Received 22 July 2008; Revised 27 November 2008; Accepted 8 January 2009

## 1. Introduction

Most low-level cross-equatorial flow in the South Asian monsoon is concentrated in a narrow band of longitudes near the East African highlands, and is often referred to as the Somali or Findlater jet (Findlater, 1969; Krishnamurti and Bhalme, 1976). This jet turns anticyclonically in the Northern Hemisphere to become the westerlies that sweep over India during boreal summer, with peak low-level wind speeds typically observed near  $10^\circ\text{N}$  off the east coast of Somalia.

Like the monsoon, the Somali jet undergoes a seasonal cycle, with northward cross-equatorial flow starting in April over the ocean east of Africa, then shifting westward in May to become zonally focused near the East African highlands (Krishnamurti and Bhalme, 1976). In June, the northern branch of zonal flow associated with the jet shifts poleward and abruptly increases in speed to become the low-level monsoon westerlies. Here we distinguish between the peak southerly winds that flow across the Equator, which we call the cross-equatorial jet, and the intense southwesterlies over the off-equatorial Arabian Sea, which we call the southwesterly jet.

The rapid increase of wind speeds in this southwesterly jet is one of the most dramatic pieces of evidence for the abrupt onset of the South Asian monsoon. We define ‘abrupt’ or ‘rapid’ relative to the seasonal cycle of insolation: an abrupt event has a time series that evolves faster than can be explained by a linear response to the insolation forcing. Given that Fourier harmonics with frequencies higher than that of the semiannual account for much less than 1% of the variance of incoming solar radiation (Weickmann and Chervin, 1988), comparing the first two seasonal harmonics of insolation to the time series of interest is one way to quantify the degree to which an event is abrupt (this is done explicitly for the Somali jet in section 3 below). Note that in addition to accounting for such a small fraction of the variance of the insolation forcing, the third seasonal harmonic has its highest amplitude in the extratropics. If the meridional gradient of insolation is instead taken as the relevant forcing, the annual harmonic becomes even more important relative to the semiannual in the tropics and subtropics, and the third harmonic retains its small amplitude. Using data from a field campaign in 1979, Krishnamurti *et al.* (1981) found that the kinetic energy of the 850 hPa horizontal wind over the Arabian Sea increased from its mean winter to its mean summer value over a single week prior to the start of monsoon rains in central India, which easily qualifies as abrupt by the above definition. The abrupt

\*Correspondence to: W. R. Boos, Dept. of Earth and Planetary Sciences, 24 Oxford Street, Harvard University, Cambridge, MA 02138, USA. E-mail: billboos@alum.mit.edu

onset of the southwesterly jet has also been documented in scatterometer data by Halpern and Woiceshyn (1999), who showed that surface wind speeds in this jet increased to their summer mean over a two-week interval in 1997, with peak values exceeding  $16 \text{ m s}^{-1}$ .

Despite the close association of the start of summer monsoon rains over India with the onset of the jet, no comprehensive multi-year study of jet onset itself has, to our knowledge, been published. Halpern and Woiceshyn (2001) verified the close association between jet intensification and the start of Indian monsoon rainfall, but they focused on interannual variations in the date of onset and did not present any sort of composite time series for the seasonal intensification. Krishnamurti *et al.* (1981) and Halpern and Woiceshyn (1999) examined only single years of jet onset. Compiling a composite picture of how winds and other variables evolve during the onset of the jet is one of the main tasks of this paper.

The other main task is to examine these composites in a convective quasi-equilibrium (QE) framework (e.g. Emanuel *et al.*, 1994) that takes the distributions of cumulus heating and pressure as part of the solution, rather than as the forcing. Previous studies of the structure of the Somali jet have employed numerical models in which the distributions of either pressure (Krishnamurti and Wong, 1979) or convective heating (e.g. Rodwell and Hoskins, 1995) were prescribed as forcings. While such studies have provided valuable insight on certain aspects of the dynamics, they presuppose a forcing which cannot truly be regarded as external. Ideally, the structure and evolution of the jet would be determined, and dynamically understood, given only the distributions of insolation and topography, and perhaps sea surface temperature (SST) if two-way ocean coupling is not considered. This paper is only a first step toward such a goal, as we limit our focus to observations and do not attempt to obtain the jet as a solution of a model system.

Studies concerned with the seasonal evolution of the Somali jet are typically framed in terms of the onset of the South Asian summer monsoon, and consider the evolution of the jet as part of a broader-scale circulation. It is possible that monsoon winds and precipitation would exhibit an abrupt seasonal onset even if the East African highlands did not serve to zonally focus the low-level flow. Indeed, an off-equatorial surface westerly jet is a characteristic feature of axisymmetric models forced by an off-equatorial thermal maximum (e.g. Krishnamurti *et al.*, 1976; Lindzen and Hou, 1988). So any theory that successfully explains the abrupt onset of a zonally symmetric solstitial circulation might also explain the abrupt onset of the southwesterly jet. Thus, while the connection between idealized, zonally symmetric Hadley circulations and the highly three-dimensional flow in monsoons may in some ways seem far from obvious, flow in the Somali jet may provide such a connection. During boreal summer, about half of the global low-level, cross-equatorial mass flux passes through the region associated with the Somali jet, which comprises only 10% of the Earth's circumference (Findlater, 1969). In this paper we do not seek to comprehensively evaluate previous theories for

monsoon onset against observations, but instead to use observations to characterize the concurrent evolution of winds and thermodynamic variables in a QE framework. We do briefly discuss the relevance of observations to a few theories for the abrupt onset of monsoons, including those that involve wind–evaporation feedback (Numaguti, 1995; Boos and Emanuel, 2008a), symmetric instability (e.g. Krishnakumar and Lau, 1997), and nonlinear transitions of angular momentum conserving circulations (e.g. Plumb and Hou, 1992).

The next section outlines the data used in this study, and is followed by the introduction of a dynamical index of Somali jet activity. This index is used to make composites of the onset of the southwesterly jet, which are then examined in the context of a QE framework. Particular attention is given to the concurrent evolution of subcloud layer entropy, free-tropospheric temperature, and sources of atmospheric moist static energy. We discuss the consistency of the composites with previous theories for monsoon onset, and conclude with a short summary.

## 2. Data

Daily-mean estimates of wind, temperature, and geopotential height on pressure surfaces for the years 1979–2005 are used from the National Centers for Environmental Prediction/National Center for Atmospheric Research (NCEP/NCAR) reanalysis (Kalnay *et al.*, 1996). We also use potential vorticity on the 350 K isentropic surface and, in order to calculate subcloud layer entropy, temperature and humidity on two low-level sigma surfaces, all from the NCEP reanalysis. The isentropic and sigma-level data are provided four times daily, and daily means are taken for use in this study.

While some details of the spatial and temporal variance of the Somali jet may be poorly represented in the low resolutions used in reanalysis datasets, no other observations of full-tropospheric behaviour seem to exist for periods of multiple years (though it should be noted that the NCEP reanalysis does assimilate satellite-derived winds). No radiosonde stations exist in the central or western Arabian Sea, or over the country of Somalia. Using scatterometer-derived surface wind speeds, Halpern *et al.* (1999) estimated the horizontal e-folding scale of the jet to be 200 km near the Equator, and found that operational analyses from the European Centre for Medium-range Weather Forecasts (ECMWF) contained errors of about 500 km in the position of the surface southwesterly jet. However, Goswami and Sengupta (2003) examined the surface southwesterly jet in two years of the NCEP reanalysis and found that, although the reanalyzed winds contained errors in the summer mean intensity and intraseasonal variance of the jet, the timing and general character of its seasonal intensification were nearly identical to that seen in scatterometer data. For this reason, it seems reasonable to use reanalyzed winds in this first attempt at creating a multi-year composite of jet intensification. There is no obvious better alternative, because the use of scatterometer data would limit our

results to surface winds over ocean, and peak meridional winds in the cross-equatorial jet are estimated to occur over the East African land surface (e.g. Findlater, 1971; Krishnamurti *et al.*, 1983).

We also examine how several other variables evolve in concert with the jet. As a proxy for deep moist convection, we use daily, satellite-estimated outgoing long-wave radiation (OLR) from the National Oceanographic and Atmospheric Administration (NOAA), interpolated in both space and time, for the same period as the reanalyzed winds (1979–2005). For surface fluxes of latent and sensible heat we employ daily data from the Objectively Analyzed Air–Sea Fluxes project (OAFlux) at the Woods Hole Oceanographic Institute (Yu *et al.*, 2004; Yu and Weller, 2007). The time range of the OAFlux dataset is limited to 1981–2002, which is what we use here. Yu *et al.* (2007) examined the statistics of the OAFlux dataset in the Indian Ocean and found that although the time mean was biased compared to *in situ* data from the Arabian Sea and Bay of Bengal, there was no major bias in the seasonal cycle of surface heat fluxes. They also stated that ocean surface heat fluxes from both NCEP and ECMWF reanalyses had little bias in their seasonal cycle over the Indian Ocean, even though they exhibited a large bias in the time mean. Finally, we estimate the net source of atmospheric moist static energy, vertically integrated from the surface to the top of the atmosphere (TOA), using energy fluxes from the NCEP reanalysis. In particular, we use the net surface fluxes of latent heat, sensible heat and radiation, together with the net radiative flux at the TOA. Because these fluxes in the NCEP reanalysis are only indirectly constrained by observations, we verify that similar patterns of change in ocean surface enthalpy fluxes occur in both the reanalysis and the more highly constrained OAFlux data. However, we use the NCEP surface fluxes to calculate the vertically integrated moist static energy source because they are presumably more energetically consistent with the NCEP radiative fluxes.

### 3. Jet index definition

We create a scalar index of jet intensity by computing the square root of twice the spatial mean kinetic energy of 850 hPa horizontal wind over the Arabian Sea, in the same spatial domain examined by Krishnamurti *et al.* (1981): 5°S–20°N; 50°E–70°E. We use the square root of the kinetic energy, rather than the kinetic energy itself, to reduce the possibility that jet intensification appears rapid only because of the use of a quadratic metric. This index can be viewed as a weighted average of 850 hPa wind speeds, with larger weights given to the stronger winds in the core of the jet, which is why we henceforth refer to this index as the ‘jet speed’.

The onset of the Somali jet is defined to occur at the start of the first three-day period, within each calendar year, during which the jet speed maintained a value more than one standard deviation above its 27-year mean. The mean onset date is 5 June, with a standard deviation

of 9 days. A composite of the seasonal intensification was formed by averaging the jet speed over all 27 years of data relative to the onset date within each year. In this composite, the jet speed takes less than two weeks to completely transition from a mean winter to a mean summer value, while a best fit of the first two seasonal harmonics takes about seven weeks to undergo the same change (Figure 1). Note that the ‘best fit’ of the seasonal harmonics was performed by finding the combination of the first two harmonics that minimized the residual in the least squares sense. Although a purely linear response would have the same weighting for these harmonics as that found in the insolation forcing, the weights of the insolation harmonics depend on latitude and on whether one chooses the insolation or its meridional gradient as the forcing. Even a calendar-based climatological mean of the jet speed intensifies faster than these seasonal harmonics, although it does so slightly more slowly than the composite. Similar results were obtained when this analysis was repeated using the domain maximum wind speed as the index instead of the square root of twice the domain mean kinetic energy.

While no radiosonde stations exist in the region of the peak Somali jet, several stations are located on islands about 500 km west of southern India, within the low-level westerlies that stretch across India to the Bay of Bengal during boreal summer (Durre *et al.*, 2006). Of these stations, only Minicoy (8.3°N, 73°E) has more than a few years of data. We have found that 850 hPa winds from Minicoy sondes exhibit the same abrupt onset behaviour seen in the closest grid cell of NCEP reanalyzed winds (not shown). This does not provide independent validation because radiosonde winds are assimilated by the NCEP model, but it does give some reassurance that our composites of the abrupt intensification of zonal wind in the southwesterly jet are not due to model artifacts alone.

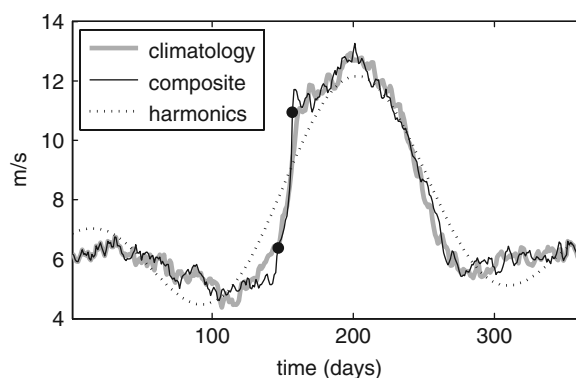


Figure 1. Annual cycle of the jet speed index in 27 years of the NCEP reanalysis. The black line represents the composite evolution relative to the date of jet onset, the grey line is a calendar-based climatology, and the dotted line is the best fit of the first two Fourier harmonics of Earth's annual cycle to the composite. Time is the number of days since 1 January, with the composite time series shifted so that jet onset occurs at day 156, the mean onset date. The two black dots are positioned at the day of onset and 10 days prior to onset.

#### 4. Wind composites

The compositing procedure described above is now used to examine how the circulation over South Asia evolves during the onset of the jet (i.e. composites were formed by averaging the specified variable over all years relative to the date of jet onset within each year). We present maps of the change in a number of variables over the 10 days preceding the onset of the jet, which might be viewed as discretized time tendencies of those variables. In these maps, we only show changes that are statistically significant at the 95% level, with significance determined at each point by an unpooled two-sample *t*-test. All of the resulting maps of changes during this 10-day period were found to be field significant at the 95% level using Monte Carlo analyses, following a procedure similar to that described in Livezey and Chen (1983). For these Monte Carlo analyses, synthetic time series were generated by randomly rearranging the dates of the raw data from which each composite was formed (i.e. phase randomization).

A composite of 850 hPa wind shows that, before the onset of the jet, Northern Hemisphere westerlies peak south of India and have a magnitude around  $5 \text{ m s}^{-1}$  over the Arabian Sea (Figure 2(a)). Easterly trades occur in the Southern Hemisphere tropics, and cross-equatorial flow occurs primarily over the east coast of Africa. During the 10 days preceding jet onset, the maximum wind speed increases by more than  $12 \text{ m s}^{-1}$  near  $10^\circ\text{N}$  over the Arabian Sea, so that the abrupt increase seen in the jet speed index is most directly a measure of off-equatorial

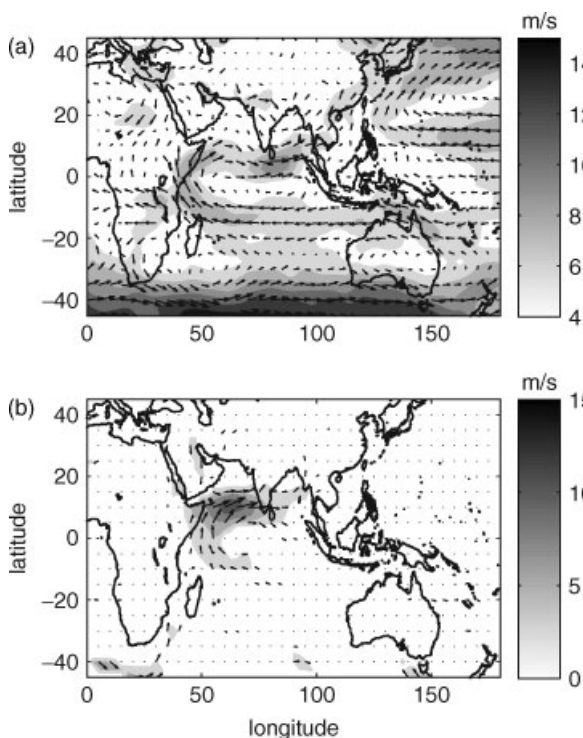


Figure 2. NCEP vector wind at 850 hPa (arrows). (a) is a composite 10 days before the date of jet onset, and (b) is the composite change in vector wind over the 10-day period preceding jet onset. In both panels, the shading denotes the magnitude of the wind vector ( $\text{m s}^{-1}$ ), not the change. Areas with surface pressure less than 850 hPa are masked out.

behaviour over ocean (Figure 2(b)). Over the same 10-day period, zonal winds also increase over southern India and the Bay of Bengal, and cross-equatorial southerlies expand eastward from the coast of Africa.

The changes in wind accompanying jet onset extend through the full depth of the troposphere. At  $10^\circ\text{N}$ ,  $60^\circ\text{E}$ , where the change in 850 hPa wind speed peaks, winds become more westerly from the surface up to about 250 hPa over the 10 days preceding jet onset (black line in Figure 3). An easterly tendency peaking at 150 hPa has a similar magnitude over this 10-day period, though at  $60^\circ\text{E}$  it is much less meridionally confined than the low-level westerly tendency (not shown). This vertical structure is roughly consistent with the first baroclinic mode used in reduced models of tropical dynamics, such as the model of Emanuel (1987) and the quasi-equilibrium tropical circulation model of Neelin and Zeng (2000). The former uses the vertical structure of a moist adiabat to define this first baroclinic mode in the horizontal wind:

$$\delta u(p) = \delta u_0 + \delta u_1 \left\{ \frac{T(p) - \bar{T}}{\Delta T} \right\}, \quad (1)$$

where  $u_1$  is then the wind speed at the top of the boundary layer,  $\Delta T$  is the difference between temperature at the top of the boundary layer and the vertically averaged, mass-weighted temperature  $\bar{T}$ , and  $\delta$  symbols are used to emphasize that we are concerned with changes in wind occurring during the onset of the jet. A vertically uniform barotropic wind speed is represented by  $u_0$ . This vertical structure is fit to the changes in zonal wind observed at  $10^\circ\text{N}$ ,  $60^\circ\text{E}$ , with the temperatures  $T$  and  $\Delta T$  assumed to be spatially and temporally invariant, and computed assuming a surface temperature of  $30^\circ\text{C}$ , a dry adiabat up to 900 hPa, and a moist pseudoadiabat between 900 hPa and 150 hPa. The best least-squares fit is obtained using  $\delta u_0 = +7.3 \text{ m s}^{-1}$  and  $\delta u_1 = +8.1 \text{ m s}^{-1}$  (grey line in Figure 3). We have not attempted to fit the wind below

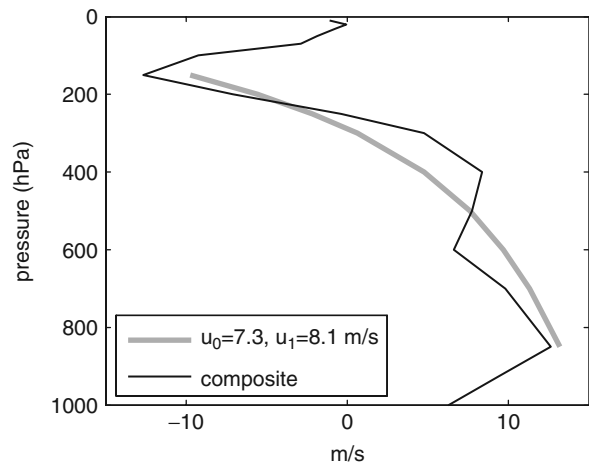


Figure 3. Vertical profile of the composite change in NCEP zonal wind at  $10^\circ\text{N}$ ,  $60^\circ\text{E}$  over the 10 days preceding jet onset (thin black line), and the best fit to this profile of two modes (one barotropic and one baroclinic) from the quasi-equilibrium framework (thick grey line). Coefficients of the fit are given in the legend.

850 hPa because the idealized QE structure does not account for momentum mixing in the boundary layer. The fit seems a decent approximation to the gross vertical structure of the composite changes, with the notable deviations of a secondary maximum at 400 hPa and a secondary minimum at 600 hPa. The barotropic wind increases by nearly as much as the baroclinic wind, suggesting that the convergence of zonal momentum into the jet may be important (see discussion by Boos and Emanuel, 2008a), although zonal pressure gradients could also play a role.

The meridional wind also exhibits a baroclinic structure, although most low-level flow is concentrated in the cross-equatorial jet. Ten days before jet onset, the meridional wind averaged between 5°N and 5°S shows peak cross-equatorial southerlies of  $10 \text{ m s}^{-1}$  at 42°E and 925 hPa, adjacent to the East African highlands (Figure 4(a)). This is consistent with the location and intensity of peak cross-equatorial winds obtained by flight surveys (Findlater, 1972; Hart *et al.*, 1978), bearing in mind that winds and surface pressure in the NCEP data represent averages over horizontal grid boxes several hundred kilometres in width. Secondary maxima of southerly cross-equatorial flow exist near the mountains of Sumatra, Borneo and New Guinea, consistent with the analysis of scatterometer-derived surface winds by Chang *et al.*

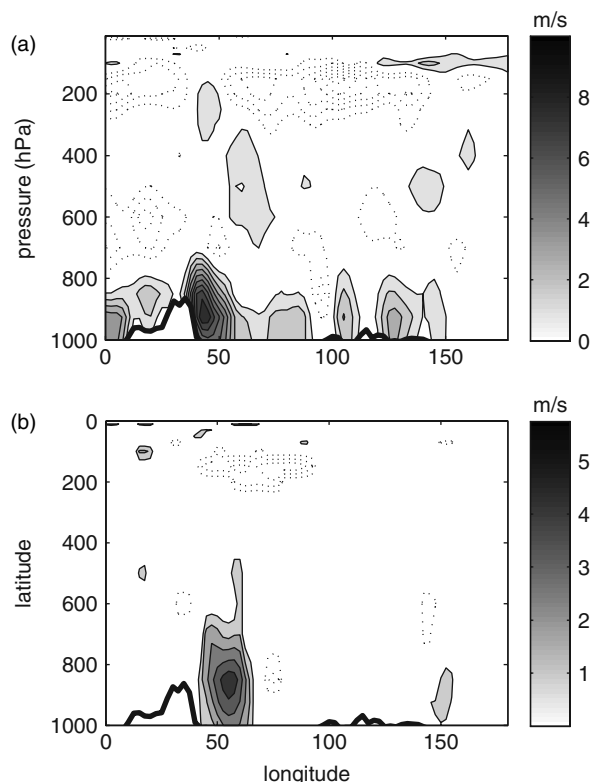


Figure 4. Vertical sections of the composite NCEP cross-equatorial flow (the meridional wind averaged between 5°S and 5°N): (a) 10 days before jet onset and (b) the change over the 10 days preceding jet onset. Solid contours with shading denote positive values (northward flow or an increase in northward flow) and dotted contours negative values. The contour interval is  $1 \text{ m s}^{-1}$  with the zero contour omitted. The thick black line denotes elevated topography (i.e. surface pressures less than 1000 hPa).

(2005). Upper-level northerlies stretch from the western Indian Ocean to the West Pacific, and there is at least a hint of a secondary maximum in southerlies near 400 hPa, similar to the secondary maximum in the zonal wind increase seen in Figure 3.

The increase in southerly flow that occurs over the 10 days before jet onset is centred near 55°E, well separated from the East African highlands (Figure 4(b)). This increase in southerlies also peaks at a slightly higher altitude and extends deeper into the free troposphere than the topographically bound flow. Upper-tropospheric northerlies also intensify from East Africa to the Bay of Bengal over this 10-day period. The rapid onset of the Somali jet should thus be thought of as an increase in off-equatorial southwesterlies over the Arabian Sea and an eastward expansion of cross-equatorial flow over the western Indian Ocean; it is not a rapid increase in the flow immediately adjacent to the East African highlands, at least in these reanalyzed winds.

The slower evolution of the core of the topographically bound cross-equatorial jet can be seen in a composite time series of the southerly cross-equatorial mass flux, integrated vertically through the troposphere and zonally between 38.75°E and 48.75°E, longitudes that encompass the peak flow immediately adjacent to the East African highlands (Figure 5). Rapid intensification synchronous with jet onset is instead seen in the eastern periphery of the cross-equatorial jet, between 48.75°E and 71.25°E. These two regions, which we refer to as the core and periphery of the cross-equatorial jet, each account for about one-quarter of the mass flux in the zonal mean cross-equatorial Hadley cell during boreal summer, consistent with the estimate by Findlater (1969) that flow between 35°E and 75°E makes up about half the global low-level mass flux during boreal summer. The fraction of zonal mean cross-equatorial flow associated with the abrupt onset of the southwesterly jet is thus at most 25%. The influence of this abrupt intensification on indices of

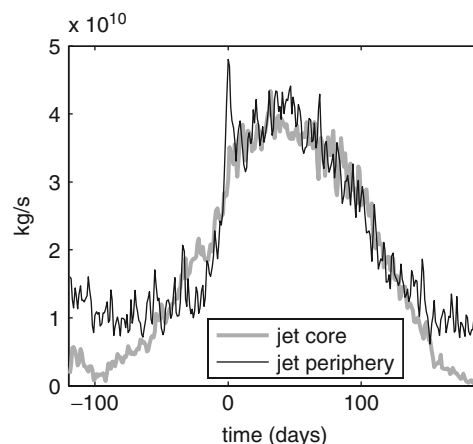


Figure 5. Composite evolution of the northward cross-equatorial mass flux in the NCEP reanalysis, integrated vertically through the troposphere and zonally, for the core of the cross-equatorial jet (38.75°E–48.75°E, grey line), and the eastern periphery of this jet (48.75°E–71.25°E, black line). Time is the number of days after jet onset.

zonal mean flow may be reduced by the fact that some low-level northerly return flow seems to occur east of the jet periphery (around  $75^{\circ}\text{E}$ , as seen in the bottom panel of Figure 4), consistent with the southward turning of the jet discussed by previous authors (e.g. Rodwell and Hoskins, 1995). Together, these findings may explain why Dima and Wallace (2003) did not find any abrupt signal of monsoon onset in a scalar index of the zonal mean Hadley circulation, despite the strong projection of South Asian monsoon flow on the boreal summer Hadley circulation.

## 5. Thermodynamic composites

The composites discussed above show that the onset of the southwesterly jet is associated with large increases in both the zonal and meridional wind over ocean. These changes, which have a strong baroclinic component, are accompanied by an increase in deep convective activity, as evidenced by a reduction in OLR over the 10 days preceding jet onset that peaks at more than  $70 \text{ W m}^{-2}$  over the Arabian Sea, and stretches across India into the northern Bay of Bengal (Figure 6). This change in OLR is similar to that described by previous authors for the onset of the Indian monsoon (e.g. Li and Yanai, 1996; Webster *et al.*, 1998), and supports the association of the start of Indian monsoon rains with the onset of the southwesterly jet.

As noted in the introduction, previous studies of the structure of the Somali jet have specified either cumulus heating or pressure gradients as forcings (e.g. Krishnamurti and Wong, 1979; Rodwell and Hoskins, 1995). The OLR composite just discussed shows that deep convection evolves in concert with the southwesterly jet, making it difficult, at best, to treat a convective heating as an external forcing. This section examines the onset of the Somali jet in a QE framework. In a state of QE, the rate of change of convective available potential energy is nearly zero when compared to the tendencies of available potential energy produced by large-scale processes such

as radiation and surface heat fluxes. In the first part of this section we use the particular QE framework reviewed by Emanuel *et al.* (1994), in which moist convection maintains the vertical temperature structure of the free troposphere near that of a moist adiabat, with the temperature of that adiabat at cloud base consistent with the entropy of the subcloud layer. In the second part of this section we examine composites of the vertically integrated source of atmospheric moist static energy; while such an examination does not explicitly require an assumption of QE, it is consistent with QE thinking in that convection does not serve as a source of moist static energy and vertical velocities must be diagnosed from something other than convective latent heating. In general, we seek to view the changes in convection, geopotential and wind that accompany jet onset as part of a convectively coupled response to the seasonally evolving radiative fluxes and surface boundary conditions. We do not assume the validity of a QE state, which might be a questionable practice especially over a land surface that extends into the subtropics, but instead attempt to generate some physical insight in the process of examining the consistency of observations with such a hypothesized state.

### 5.1. Assessment in a quasi-equilibrium framework

One of the simplest statements of convective QE is that changes in the subcloud layer entropy  $s_b$  are matched by equal changes in  $s^*$ , the saturation entropy of the free-tropospheric convecting layer (e.g. Emanuel, 1987):

$$\delta s^* = \delta s_b \quad (2)$$

This relationship is expected to hold only in convecting regions, while in nonconvecting regions  $s^*$  can decouple from  $s_b$ . This is an important point because in strong, thermally direct circulations, subsidence can suppress deep convection and thus produce large areas where (2) is not expected to hold. However, given that the ascending regions in such circulations should occur in the regions of highest  $s_b$  and  $s^*$ , (2) amounts to the condition that the peaks of  $s_b$  and  $s^*$  be collocated.

If monsoon circulations are found to be consistent with a QE framework, such a framework might help in understanding the mechanisms that set both the seasonal evolution and seasonal mean behaviour of monsoons. For example, Emanuel (1995) showed that, in QE, a sufficient condition for the onset of thermally direct, deep-tropospheric flow can be expressed in terms of horizontal gradients of  $s_b$  (Emanuel, 1995). When this condition is met (i.e. when  $s_b$  gradients are supercritical), the  $s^*$  and  $s_b$  peaks are expected to be coincident, and  $s^*$  will be relaxed toward the critical distribution by the large-scale circulation. This is simply an extension to a moist atmosphere of the dynamical control on free-tropospheric temperatures found in theories of axisymmetric, angular momentum conserving circulations (e.g. Held and Hou, 1980). In idealized models of monsoons, Privé and Plumb (2007b) found that zonal asymmetries introduced numerical complexities to such axisymmetric theories, but that

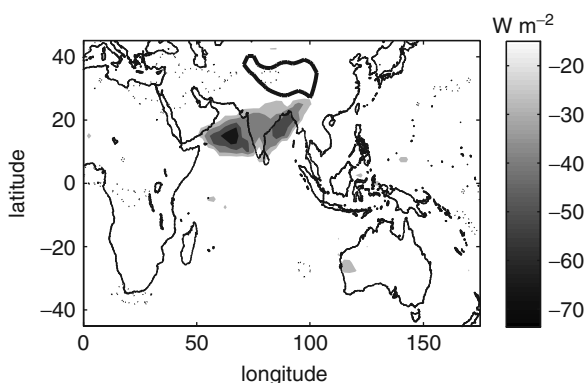


Figure 6. Composite change in NOAA OLR over the 10 days preceding jet onset. Shading denotes a reduction in OLR, and dotted contours an increase. The contour interval is  $15 \text{ W m}^{-2}$ , with the zero contour omitted. The thick black line surrounds regions with surface pressures lower than 700 hPa (i.e. the Tibetan Plateau).

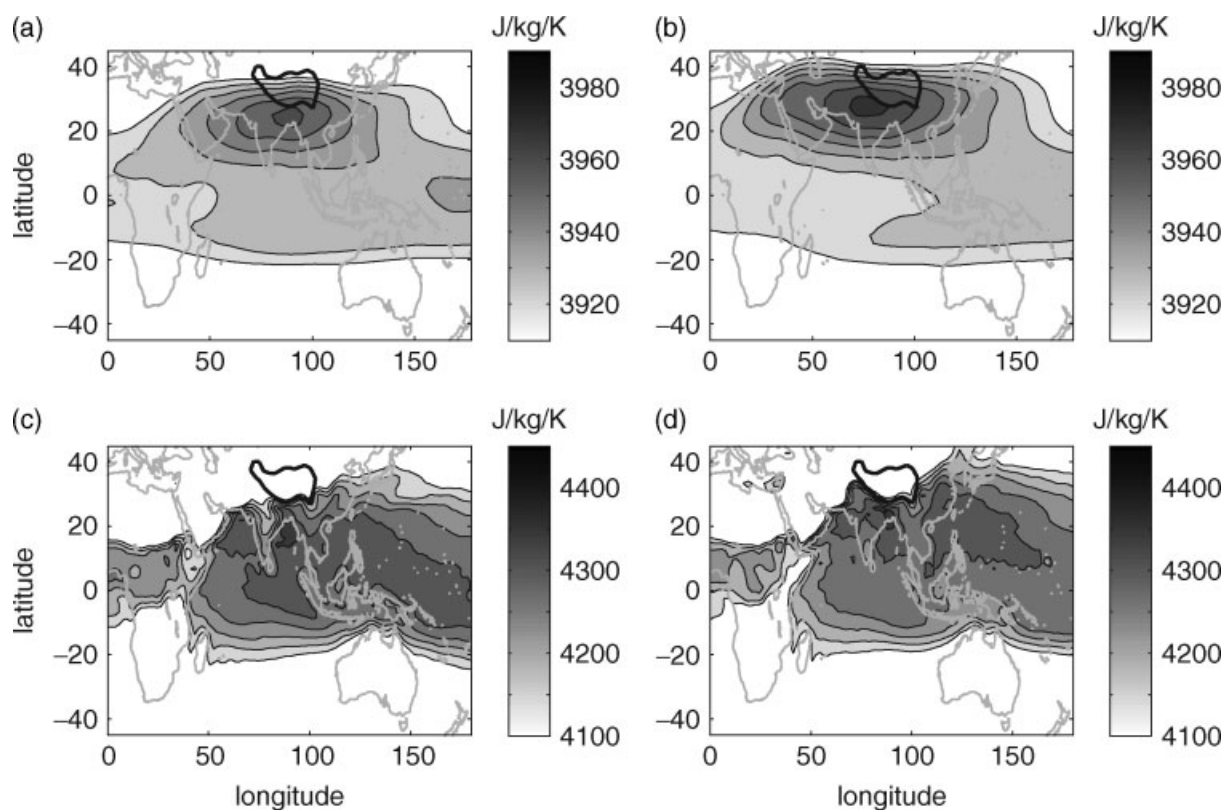


Figure 7. Calendar-based climatological means of the NCEP saturation moist entropy averaged between 450 hPa and 175 hPa in (a) June and (b) July. (c, d) is as (a, b), but for the NCEP moist entropy averaged over the 0.9821 and 0.9644 sigma levels. In (a, b), the contour interval is  $10 \text{ J kg}^{-1} \text{ K}^{-1}$  with shading starting at  $3920 \text{ J kg}^{-1} \text{ K}^{-1}$ . In (c, d), the contour interval is  $50 \text{ J kg}^{-1} \text{ K}^{-1}$  with shading starting at  $4150 \text{ J kg}^{-1} \text{ K}^{-1}$ .

the position of the  $s_b$  peak still served to delineate the poleward boundary of the monsoon circulation, with maximum ascent and precipitation occurring just equatorward of this peak (also Privé and Plumb, 2007a). This is consistent with the treatment of zonal asymmetries introduced by Emanuel (1995) in his theory of moist, thermally direct flow that conserves absolute angular momentum in the free-troposphere. These and other ideas will be discussed in the context of the composites presented below.

As an estimate of  $s^*$ , we compute the mass-weighted vertical mean saturation moist entropy from NCEP temperatures between 450 hPa and 175 hPa, using the lower bound of 450 hPa to minimize any contribution of boundary-layer air over the Tibetan Plateau to the vertical mean. As an estimate of  $s_b$ , we compute the average moist entropy on the 0.9821 and 0.9644 sigma surfaces of the NCEP reanalysis. These terrain-following surfaces are the two model levels just above the lowest sigma level of 0.9950, and lie within the bottom 50 hPa of the atmosphere. While it may be appropriate to define a deeper subcloud layer in regions with extensive vertical mixing of entropy by shallow cumulus, it is not clear whether such shallow mixing is prevalent in the South Asian summer monsoon, especially at the time of its onset. Entropies on sigma surfaces, rather than on any particular pressure surface, are used for  $s_b$  in order to avoid excluding the Tibetan Plateau, which has long been thought to play a central role in the thermodynamics of the South Asian monsoon (e.g. Flohn, 1974; Hahn and Manabe, 1975).

Before examining the detailed changes that accompany the onset of the Somali jet, we examine the summer mean entropy distributions to provide some sense of the background state. In a calendar-based June climatology,  $s_b$  peaks over the northern Bay of Bengal and generally has higher values over ocean than land (Figure 7). The peak  $s^*$  during June is centred about 500 km poleward of the  $s_b$  peak, over the northern coastal regions of the Bay of Bengal. The distribution of  $s^*$  is much smoother than that of  $s_b$ , consistent with the expectation that dynamics will constrain horizontal gradients of tropical free-tropospheric temperature to be fairly weak. As discussed above, one simple check on the consistency of these distributions with QE is that the maxima of  $s_b$  and  $s^*$  are collocated; given that the spatial offset of these maxima during June is about two grid cells of the NCEP data, this requirement seems to be at least approximately satisfied. As time progresses from June to July, the  $s^*$  peak increases in magnitude and migrates northwest over the northern parts of India. The regions of high  $s_b$  shift deeper into the Northern Hemisphere in July, and the domain maximum  $s_b$  protrudes inland from the Bay of Bengal to extend along the southern edge of the Tibetan Plateau.

We computed the same entropy climatologies using the ECMWF reanalysis (ERA-40) for 1979–2002, using the same pressure levels for  $s^*$  and computing the subcloud entropy on eta level 57, which has a similar vertical position as the sigma levels chosen for the NCEP data. The  $s^*$  distributions were nearly identical to those

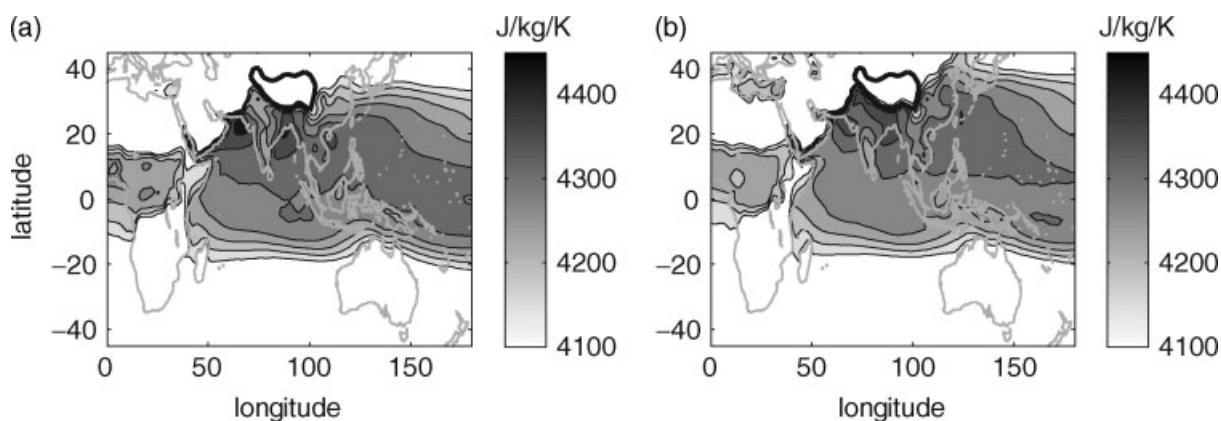


Figure 8. As Figure 7(c, d), but for the ERA-40 data for 1979–2002.

computed with the NCEP data and so are not shown here, but some notable differences were found in the  $s_b$  fields. In June, the ERA-40 data show a larger  $s_b$  peak over the northern Arabian Sea and higher values of  $s_b$  over India (Figure 8). The  $s^*$  peak still seems to have a slight inland bias relative to these  $s_b$  maxima. In July, the tongue of high  $s_b$  air that seemed to originate in the northern Bay of Bengal is larger and extends further inland along the base of the Tibetan Plateau in the ERA-40 data than in the NCEP data. Although the contour interval in Figure 8 is too large to distinguish the precise location of the  $s_b$  peak in July, it is located on the inland portion of this tongue, closer to the  $s^*$  peak than in the NCEP data.

The climatological entropy distributions just discussed are inconsistent with the notion of the Tibetan Plateau serving as the dominant thermodynamic forcing in the South Asian monsoon. Maxima in  $s^*$  and  $s_b$  are never centred over the Tibetan Plateau, which actually has smaller values of subcloud entropy than the lower elevations immediately to its east at the same latitude. Indeed, the southern boundary of the Tibetan Plateau is largely coincident with the northern extent of the region of highest  $s_b$ . (Note that no masking is used in Figure 7 or 8;  $s_b$  over the plateau simply falls below the lowest contour value displayed.)

We suggest that the absence of an entropy peak over the plateau might be due to either surface albedo effects, or to the orographic blocking of high-entropy air transported inland from warm oceans. While  $s_b$  and  $s^*$ , in radiative–convective equilibrium, are expected to be larger over an elevated surface than over a surface at sea level with otherwise identical properties (Molnar and Emanuel, 1999), the surface properties of the Tibetan Plateau differ from those of non-elevated parts of South Asia. In particular, the average surface albedo of the plateau is higher than that of non-elevated surfaces to its east by about 0.06, as seen in the broadband short-wave surface albedos used in the International Satellite Cloud Climatology Project (ISCCP) D2 climatology for July (Rossow *et al.*, 1995; not shown). According to the calculations of Molnar and Emanuel (1999), such an albedo increase can compensate for much of the increase in radiative–convective equilibrium temperatures expected to be

achieved by elevating a surface from sea level to 600 hPa, depending on the availability of surface moisture. The ISCCP surface albedos for the Tibetan Plateau, however, are not uniformly higher than those for much of continental India, which suggests that subcloud entropies may be elevated over land south of the plateau because of horizontal advection from the adjacent ocean, with orography blocking the flow of this high-entropy air onto the plateau. This is qualitatively consistent with the subcloud entropy distributions shown in Figure 7, which have oceanic peaks with peripheries that protrude into neighbouring coastal regions. Given that humidity variations constitute a large part of variations in subcloud entropy, orographic blocking could also indirectly enhance radiative cooling over the Tibetan Plateau by reducing the long-wave opacity of the overlying atmosphere. While further work is needed to assess the relative importance of these effects in setting the distribution of entropies over South Asia, we emphasize that these entropy distributions suggest that the thermal forcing of the plateau does not play a central role in the onset of the Somali jet in a QE framework.

Turning our attention from the summer mean state to the time of jet onset, we see that 10 days before onset the highest subcloud entropies occur in a broad peak that extends from the Bay of Bengal, across the Indochina Peninsula, to the western Pacific (Figure 9(a)). Subcloud entropies are much lower over continental India, which is consistent with strong monsoon precipitation occurring over the Indochina Peninsula before the onset of the Indian monsoon (e.g. Krishnamurti, 1985). During the 10 days before jet onset, the largest subcloud entropy increase occurs just north of the Bay of Bengal in a region of strong horizontal gradients of  $s_b$  (Figure 9(b)). This increase results from the formation of the tongue of high-entropy air that penetrates inland from the Bay of Bengal in June (Figure 7(c)). Explicit calculation of entropy advection along the 0.9821 and 0.9644 sigma surfaces of the NCEP reanalysis shows that the peak increase in advection over the 10 days preceding jet onset is collocated with this peak change in  $s_b$  just north of the Bay of Bengal, but that the increase in advective tendency is an order of magnitude larger than that needed to produce the  $s_b$  change (not shown). Such a large

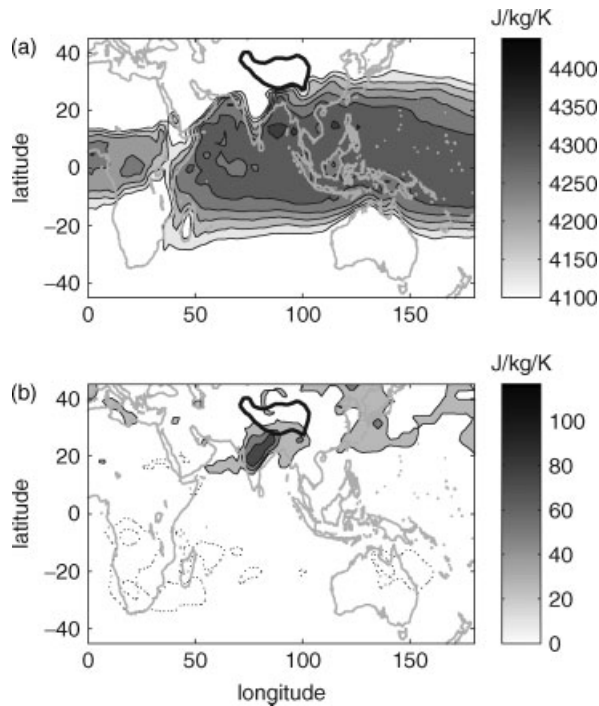


Figure 9. Composites of the NCEP moist entropy averaged over the 0.9821 and 0.9644 sigma levels. (a) shows this subcloud entropy 10 days before jet onset, with a contour interval of  $50 \text{ J kg}^{-1} \text{ K}^{-1}$  starting at  $4130 \text{ J kg}^{-1} \text{ K}^{-1}$ . (b) shows the change in subcloud entropy over the 10 days preceding jet onset, with solid contours denoting an increase, dotted contours a decrease, a contour interval of  $30 \text{ J kg}^{-1} \text{ K}^{-1}$ , and the zero contour omitted.

difference is expected in theories of subcloud layer QE, in which any time tendency of subcloud entropy results from a slight imbalance between the much larger tendencies due to surface fluxes, convective downdraughts and horizontal advection within the subcloud layer (e.g. Raymond, 1995). Similar patterns occur in the ERA-40  $s_b$  distribution, although the amplitude of the  $s_b$  increase over India extends further inland (not shown), consistent with the higher subcloud entropies seen over India in the June climatology of that dataset (e.g. Figure 8(a)).

During the 10 days before jet onset, the  $s^*$  peak is centred over the northeast coast of the Bay of Bengal, about 500 km north and east of the  $s_b$  peak (Figure 10(a)). This spatial offset is similar to that seen between the  $s^*$  and  $s_b$  peaks in the June climatology, and raises the question of whether the thermodynamic influence of a land surface might cause some deviations from the QE state denoted by (2). One possibility is that a strong diurnal cycle of convection over land renders  $s^*$  more closely in equilibrium with the daily maximum value of  $s_b$  instead of the daily mean that was used here. Examination of this possibility is left for future work. The largest increase in  $s^*$  over the 10 days before jet onset is centred along the southwest edge of the Tibetan Plateau (Figure 10(b)). This increase extends to the west in a zonally elongated structure; we discuss the similarity of this structure to a beta plume in section 6. This increase actually results from a shift to the northwest of the  $s^*$  peak and a poleward expansion of the highest

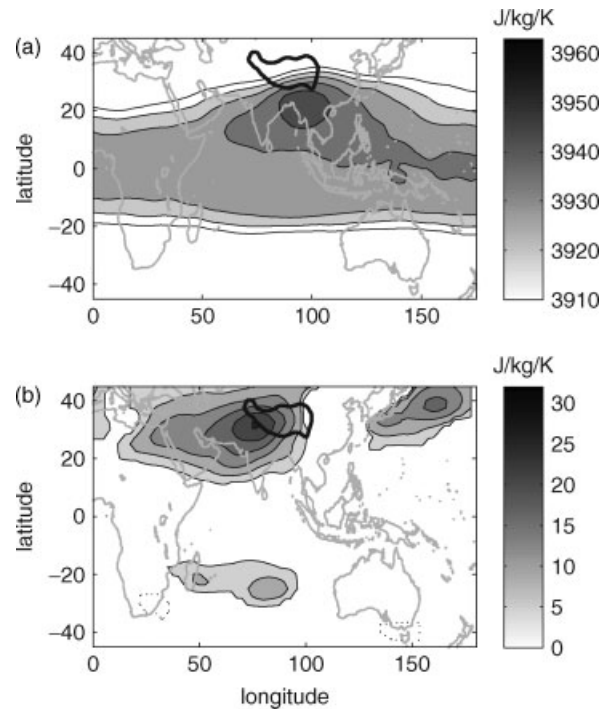


Figure 10. As Figure 9, but for the vertical mean from 450 hPa to 175 hPa of the NCEP saturation moist entropy. In (a), the contour interval is  $10 \text{ J kg}^{-1} \text{ K}^{-1}$  starting at  $3910 \text{ J kg}^{-1} \text{ K}^{-1}$ . In (b), the contour interval is  $5 \text{ J kg}^{-1} \text{ K}^{-1}$ .

free-tropospheric temperatures. On the day of jet onset, the  $s^*$  peak is centred over the northernmost edge of the Bay of Bengal (not shown), similar to its position in the June climatology. If QE holds, the change in  $s^*$  need not have the same structure as that in  $s_b$  because much of these changes occur in regions of subsidence. At 300 hPa, which is midway through the layer over which  $s^*$  was averaged and is also the level at which ascent typically peaks in this region, strong subsidence exists nearly everywhere west of the Tibetan Plateau (Figure 11(a)). This pattern of vertical motion will be discussed in a later section of this paper, together with some possible reasons for the zonally elongated structure of the increase in  $s^*$ .

Changes in  $s^*$  are dynamically relevant because they are equivalent, through hydrostatic balance, to changes in the thickness of the convecting layer (Emanuel *et al.*, 1994). That is, where the free troposphere warms it will increase in thickness and, barring any change in the vertical-mean geopotential of the free troposphere, be accompanied by a decrease in geopotential near the top of the boundary layer. The change in  $s^*$  that accompanies jet onset has sharp gradients that extend from northern Africa all the way to the eastern Tibetan Plateau (Figure 10(b)), implying an increase in balanced baroclinic flow in these regions. However, the peak decrease in 850 hPa geopotential height is centred over the Arabian Sea and has a more limited spatial extent (Figure 12(a)), which suggests that a barotropic change in geopotential does occur to oppose some of the effects of the  $s^*$  increase on the low-level geopotential. To confirm that such a barotropic change does occur, we use the vertical mean geopotential from 850 hPa to 150 hPa in the NCEP

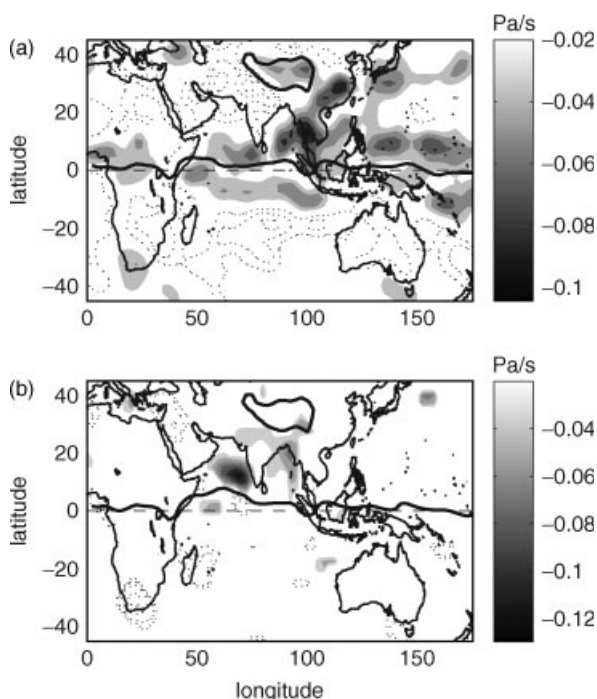


Figure 11. As Figure 9, but for the NCEP vertical velocity at 300 hPa. In both panels, shading denotes negative values (ascent or an increase in ascent), dotted contours denote positive values, and the contour interval is  $0.02 \text{ Pa s}^{-1}$  with the zero contour omitted. The horizontal dashed line represents the Equator. The thick black line near the Equator is the zero contour of 850 hPa absolute vorticity (a) 10 days prior to jet onset, and (b) on the day of jet onset.

reanalysis as an estimate of the barotropic component of the geopotential field. The composite change in this barotropic geopotential during the 10 days before jet onset does oppose the baroclinic changes implied by the increase in  $s^*$  over continental Asia and Africa, and it slightly enhances the baroclinic changes over the Arabian Sea (Figure 12(b); note that an increase in  $s^*$  corresponds to a decrease in the baroclinic component of the low-level geopotential). Although we do not explore the cause of this pattern of barotropic change in detail, we suggest that it may be related to the effects of surface drag and momentum convergence. Boos and Emanuel (2008a) discussed how, during the onset of a solstitial Hadley circulation, the spin-up of a baroclinic circulation by a thermal forcing will be accompanied by the spin-up of a barotropic circulation, due to surface drag, that opposes the baroclinic flow at low levels. In regions of strong ascent, the convergence of horizontal momentum can produce a barotropic circulation that enhances, rather than opposes, the low-level baroclinic flow. It seems reasonable to expect that such momentum convergence might occur over the Arabian Sea and Bay of Bengal, which we shall now show is where peak ascent occurs during jet onset.

The coherent increases in ascent that accompany the onset of the Somali jet are centred over the Arabian Sea just downstream of the peak southwesterly jet (Figure 11(b)). Although rates of ascent are only indirectly constrained by observations in reanalysis data, the large increase in deep ascent over the Arabian Sea is

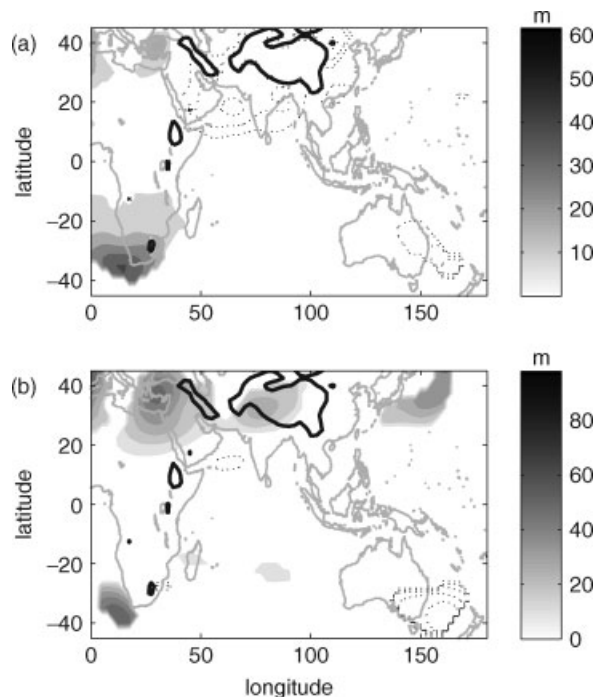


Figure 12. (a) shows the composite change in NCEP geopotential height at 850 hPa over the 10-day period preceding jet onset, and (b) the vertical mean (averaged from 850 to 150 hPa) change in geopotential height. Shading denotes an increase, dotted contours a decrease, and the zero contour is not shown. Contour interval is 10 m in both panels. Areas with surface pressures lower than 850 hPa are surrounded by the thick black line, and are masked out in (a); values within such regions in (b) were obtained using the extrapolated geopotentials provided in the NCEP reanalysis.

consistent with the simultaneous reduction of OLR in this region (e.g. Figure 6). A weaker and spatially broader increase in ascent is centred over the northern Bay of Bengal, extending up to the base of the Tibetan Plateau and over northern India. Before jet onset, peak ascent is centred over the near-equatorial ocean, the Indochina Peninsula and southeastern China. Strong subsidence occurs to the west of the ascending regions, consistent with Rossby wave dynamics (Gill, 1980; Rodwell and Hoskins, 1996). The strong subsidence to the west of the Tibetan Plateau 10 days before jet onset is not accompanied by an equally strong region of ascent over the plateau itself.

In summary, maxima of  $s_b$  and free-tropospheric  $s^*$  are nearly collocated during summer, suggesting that QE may provide a valid description of the South Asian monsoon. During the 10 days before jet onset, the pool of high-entropy air that was previously confined to oceanic regions and the Indochina Peninsula expands inland over continental India. The large increase in low-level southwesterlies over the Arabian Sea seems to be in balance with the increase in  $s^*$  that is centred over continental Asia; dynamical changes at low levels over continental regions are largely cancelled by the spin-up of barotropic flow. It is not clear whether the inland expansion of high- $s_b$  air over India is caused by the onset of the jet, or whether both processes simply occur as part of the spin-up of the larger-scale monsoon circulation.

## 5.2. Assessment of the moist static energy budget

The statement of convective QE given by (2) allows for a balanced baroclinic circulation to be inferred from diagnosis of the entropy field, but does not allow for direct determination of vertical motion. Because of the weak free-tropospheric temperature gradients in the Tropics, vertical motion can be diagnosed by calculating the adiabatic cooling needed to balance a given diabatic heating, but such a diagnostic relation is of little use if one does not wish to assume the location and intensity of deep convection *a priori*. For this reason, we examine changes in vertical motion in the context of the vertically integrated budget of moist static energy, using methodology similar to that of Neelin and Held (1987). The vertically integrated budget for moist static energy,  $h$ , is

$$\left\langle \frac{\partial h}{\partial t} \right\rangle + \langle \mathbf{v}_h \cdot \nabla h \rangle + \left\langle \omega \frac{\partial h}{\partial p} \right\rangle = Q, \quad (3)$$

where angle brackets denote mass-weighted vertical integrals from the surface to the TOA, and  $\mathbf{v}_h$  is the horizontal wind. Here  $Q$  is the net source of moist static energy in an atmospheric column, which is equal to the net surface enthalpy flux plus the net atmospheric radiative flux convergence. Consider the idealized case where the local time tendency and horizontal advection terms are negligible compared to other terms in the balance, and the vertical velocity has a constant vertical structure given by the function  $\Omega(p)$

$$\omega(p) \equiv \bar{\omega} \Omega(p), \quad (4)$$

where  $\bar{\omega}$  is a scalar. Under such conditions, the vertical velocity is linearly related to the net column source of moist static energy:

$$\bar{\omega} = \frac{Q}{\left\langle \Omega(p) \frac{\partial h}{\partial p} \right\rangle}. \quad (5)$$

Rather than compute all the terms in the full budget (3), we study the co-evolution of  $Q$  and vertical velocity during the process of jet onset, and examine after the fact whether the approximation (5) seems to hold. Diagnosis of the seasonal cycle of the gross moist stability  $\left\langle \Omega(p) \frac{\partial h}{\partial p} \right\rangle$  is left for future work, although it is recognized that this quantity may vary considerably in both space and time. Elevated terrain, in particular, might be expected to alter  $\partial_p h$  to the degree that surface temperatures and humidities are invariant with surface height (although these quantities are evidently not invariant as one ascends from sea level to the surface of the Tibetan Plateau, as shown in the previous section). Also, monsoon onset is sometimes conceptualized as the transition from a shallow, thermally direct circulation that is capped by subsidence to a circulation with full-tropospheric ascent. While such a process would involve a large change in the vertical structure function  $\Omega$ , the region of shallow ascent is typically posited to occur over land due to the formation of a deep dry boundary layer

(e.g. Xie and Saiki, 1999). Thus, (5) may hold over ocean, if not over land, a scenario that will prove consistent with the composites presented below.

The moist static energy source  $Q$  is computed by summing the surface enthalpy flux and the net atmospheric radiative flux convergence, both obtained from the NCEP reanalysis. Although these NCEP estimates are only indirectly constrained by observations, they are used here because they provide values over both land and ocean (unlike the OAFflux dataset, which is presented later for comparison), and because they provide a dataset expected to be at least roughly internally consistent in its energetics. Such consistency would be lacking if, say, the OAFflux surface enthalpy fluxes were combined with an independent estimate of radiative flux convergence. Ten days before jet onset, this NCEP  $Q$  field shows a broad region of net heating (i.e.  $Q > 0$ ) over East Asia, as well as sharper off-equatorial maxima in the Indian Ocean near the peak low-level zonal winds (Figure 13(a)). Over the 10 days before jet onset,  $Q$  increases by almost  $200 \text{ W m}^{-2}$  at the location of the peak southwesterly jet (Figure 13(b)), an increase that is larger than any of the maxima in the pre-existing basic state. A reduction in the atmospheric radiative flux divergence accounts for about one quarter of this increase in  $Q$ , with the remainder comprised almost entirely of the surface latent heat flux (not shown). The fact that vertical velocity (Figure 11) and  $Q$  both show sharp increases over the eastern Arabian Sea that are nearly collocated suggests that (5) may hold in this region, at least to a first approximation.

The change in  $Q$  over nearly all land surfaces during the 10 days before onset is less than  $20 \text{ W m}^{-2}$ , likely

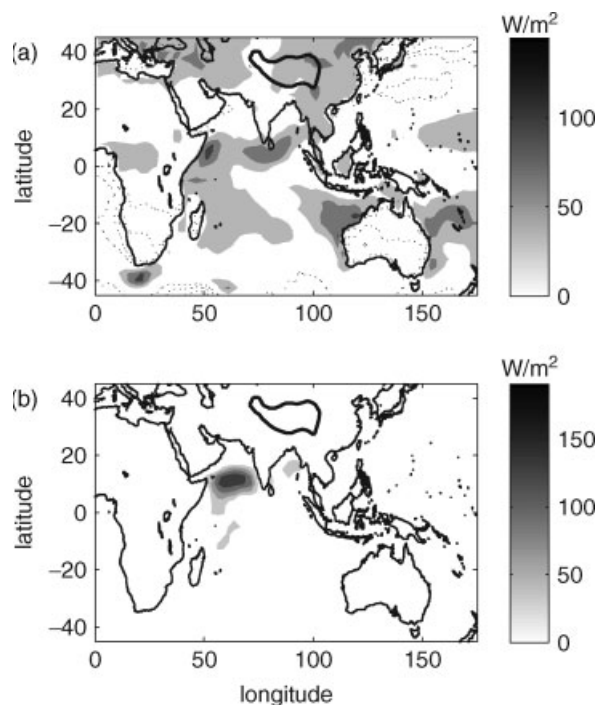


Figure 13. As Figure 9, but for the vertically integrated atmospheric source of moist static energy in the NCEP reanalysis. In both panels the contour interval is  $40 \text{ W m}^{-2}$ .

because of the constraint that the relatively small land surface heat capacity places on the surface energy budget. The energy budget for a near-surface soil layer is

$$C_s \frac{\partial T_s}{\partial t} = -E - R_s + G, \quad (6)$$

where  $C_s$  is the heat capacity of the layer,  $E$  the surface enthalpy flux into the atmosphere,  $R_s$  the net upward surface flux of radiative energy, and  $G$  the upward flux of heat from lower soil layers. This budget can also be written

$$Q = R_{\text{TOA}} + G - C_s \frac{\partial T_s}{\partial t}, \quad (7)$$

where  $R_{\text{TOA}}$  is the net downward radiative energy flux at TOA. If we consider only a thin near-surface soil layer and average over a sufficiently long time period for the last term to be negligible (e.g. several days), then changes in  $Q$  must be balanced by changes in the ground heat flux or in the radiative balance at TOA.

While large abrupt changes in the ground heat flux or in the TOA radiative balance over land could theoretically occur during monsoon onset, evidence for such changes does not exist in composites of NCEP data for jet onset. Averaged over the South Asian longitudes of 60–110°E,  $Q$  goes through a fairly smooth seasonal cycle over the predominantly terrestrial region of 20–40°N, which includes the Tibetan Plateau (Figure 14(a)). In this region,  $Q$  is about 20 W m<sup>-2</sup> less than the TOA flux

during boreal summer, presumably due in large part to ground heat flux associated with the warming and melting of fairly deep layers of snow, ice and frozen soil. Over the predominantly oceanic domain of 0–20°N, 60–110°E,  $Q$  does increase abruptly by about 30 W m<sup>-2</sup> over the 10 days before jet onset, mostly because of the large increase over the Arabian Sea. When these same regional averages are applied to  $\omega$  at 300 hPa, a fairly linear relationship is seen between  $\omega$  and  $Q$  for the oceanic region (0–20°N, 60–110°E) during the 100 days surrounding jet onset (compare black lines in Figures 14(a) and (b)). A somewhat weaker abrupt increase in ascent is also seen in the land region (20–40°N, 60–110°E), and the fact that no similar abrupt change occurs in  $Q$  for this region implies that abrupt changes must occur in the gross moist stability or in the horizontal advection or local time tendency of  $h$ . A change in the vertically integrated  $h$  advection would be consistent with the increase in  $s_b$  advection discussed in the previous section, since horizontal  $h$  gradients in the free troposphere are expected to be much weaker than those in the boundary layer.

To provide some sense of the accuracy of the distribution of  $Q$  calculated from the NCEP reanalysis, we examine the ocean surface enthalpy flux from the OAFflux dataset. Ten days before jet onset, this flux peaks in a broad, zonally elongated band near 20°S (Figure 15(a)). A weaker secondary maximum exists just north of the Equator in the western Indian Ocean, where low-level westerlies peak. In comparison, the distribution of the pre-onset surface enthalpy flux in the NCEP reanalysis is similar over the southern Indian Ocean, but is larger than the OAFflux values by about 60 W m<sup>-2</sup> over the northern Indian Ocean (not shown). Over the 10 days before jet

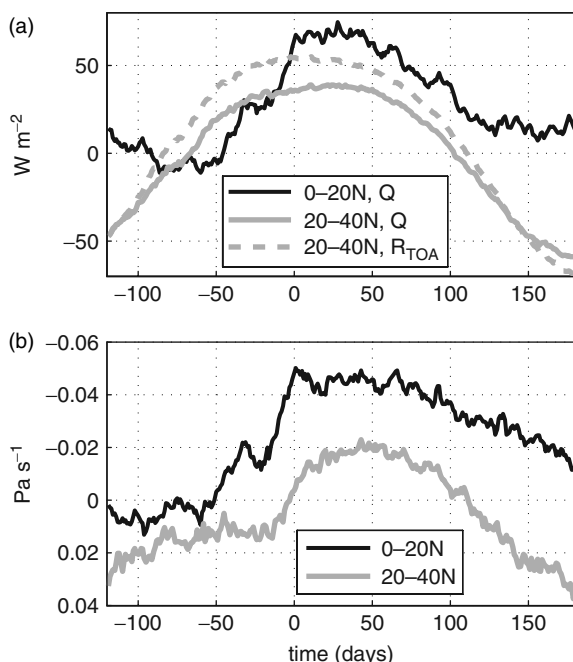


Figure 14. Composite evolution of (a) the vertically integrated atmospheric moist static energy source in the NCEP reanalysis and (b) the NCEP vertical velocity at 300 hPa. All quantities are spatial means from 60 to 110°E, with the solid grey line denoting a mean from 20 to 40°N (a predominantly land domain) and the black line a mean from 0 to 20°N (predominantly ocean). The dashed grey line in (a) denotes the net radiative flux at the top of the atmosphere for 20–40°N. Time is the number of days after jet onset.

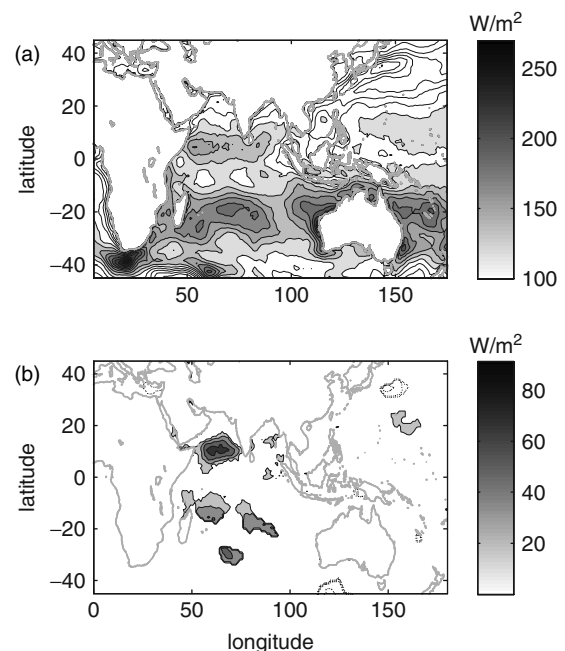


Figure 15. As Figure 9, but for the ocean surface enthalpy flux from the OAFflux project. Contour interval is 20 W m<sup>-2</sup> in both panels, with shading in (a) starting at 100 W m<sup>-2</sup>.

onset, the OAFlux dataset shows an increase in the surface enthalpy flux that peaks at more than  $80 \text{ W m}^{-2}$  in the Arabian Sea at the location of the peak southwesterly jet (Figure 15(b)). A weaker increase also occurs over the southern Indian Ocean. The increase in the Arabian Sea is consistent with measurements collected over the course of one year from a surface mooring deployed along the climatological axis of the southwesterly jet (Weller *et al.*, 1998). Compared to these OAFlux values, the NCEP reanalysis overestimates the increase in Arabian Sea surface enthalpy fluxes during the 10 days preceding jet onset by almost a factor of two, although it does seem to have the correct spatial and temporal pattern. Although the change in NCEP surface enthalpy fluxes is not shown explicitly, it can be inferred by knowing that about one quarter of the  $200 \text{ W m}^{-2}$  increase in  $Q$  over the Arabian Sea shown in Figure 13 results from a decrease in atmospheric radiative flux divergence, as stated above.

We briefly note that, in both the NCEP and OAFlux datasets, the increase in surface enthalpy fluxes over the Arabian Sea that accompanies jet onset is followed by a decrease to a more moderate summer mean value (not shown). This is consistent with the mooring data presented by Weller *et al.* (1998), which showed ocean evaporation peaking shortly after the onset of the southwesterly jet, then decreasing as summer progressed due to both a reduction in SST and an increase in the relative humidity of surface air over the Arabian Sea. This would be consistent with a wind–evaporation feedback playing an important role in the abrupt onset of the Somali jet (see discussion below), but being damped by ocean cooling in its effect on the summer mean circulation.

## 6. Discussion

### 6.1. Wind–evaporation feedback

The fact that the large increases in low-level wind, surface enthalpy fluxes and deep ascent (e.g. Figures 2, 11 and 15) are both concurrent and collocated is suggestive of a wind–evaporation feedback playing a central role in the high-amplitude intensification of the southwesterly jet. (Here we use the term wind–evaporation feedback synonymously with wind-induced surface heat exchange (WISHE), assuming that the latent component of any WISHE feedback dominates over the tropical ocean.) Numaguti (1995) showed that the wind-dependence of surface evaporation in an aquaplanet general circulation model (GCM) caused the precipitation peak to jump discontinuously from the Equator to about  $15^\circ\text{N}$  as the SST maximum was slowly moved northward from the Equator. This abrupt poleward shift in the precipitation maximum was accompanied by a large, collocated increase in surface evaporation, and thus in the vertically integrated atmospheric moist static energy source. Figure 11 shows a considerably smaller poleward shift of the ascent peak, from about  $5^\circ\text{N}$  to  $10^\circ\text{N}$  over the Arabian Sea, while over the Bay of Bengal the region of ascent simply expands, rather than shifts poleward. In contrast to the

meridionally migrating SST maximum used as a forcing by Numaguti (1995), Boos and Emanuel (2008a) examined the response of axisymmetric aquaplanet models to a spatially-fixed, off-equatorial SST anomaly that varied in amplitude and sign in a seasonal cycle. For such an off-equatorial forcing, they found that the off-equatorial ascent zone intensified abruptly with little meridional migration because of a positive feedback between the wind-driven surface enthalpy flux, deep ascent, and the low-level rotational flow needed to balance convergence into the ascent region.

Boos and Emanuel (2008a) also discussed how surface drag in Hadley circulations can strongly damp any wind–evaporation feedback by producing a barotropic wind that nearly cancels the baroclinic component of low-level flow in most regions. In their models, a positive wind–evaporation feedback occurred only when barotropic westerlies were created by the convergence of zonal momentum into an off-equatorial ascent zone. The previous section showed that the changes in zonal wind near the Arabian Sea ascent zone were decently described by the superposition of a barotropic and baroclinic mode that constructively interfered to produce strong westerlies at low levels (e.g. Figure 3). The creation of barotropic westerlies by momentum convergence into an off-equatorial ascent zone is generally expected to occur even without a wind–evaporation feedback given a sufficiently strong circulation, so the relevant issue is whether the large increase in surface enthalpy flux over the Arabian Sea alters the dynamics or simply occurs as a passive response. We suggest that a causal role for the enhanced surface enthalpy fluxes is indicated by the fact that the abrupt increases in ascent and  $Q$  are nearly collocated (as shown in Figures 11 and 13) while the peak free-tropospheric temperature is positioned considerably further poleward. The large increase in ascent that occurs over the Arabian Sea during jet onset is located about  $10^\circ$  of latitude south of the  $s_b$  and  $s^*$  peaks (cf. Figures 11 and 7), a much larger offset than is seen in the aquaplanet models of Numaguti (1995) or Boos and Emanuel (2008a), or in the dry models of Plumb and Hou (1992) or Lindzen and Hou (1988). This relatively large offset could be due to the fact that wind–evaporation feedback is not expected to operate over land, due to its relatively small thermal inertia. That is, even if the  $s_b$  and  $s^*$  peaks were clearly centred deep over a continental interior, any wind–evaporation feedback, and thus any associated abrupt increase in ascent, must occur over ocean. The South Asian monsoon may be in a regime where the land surface thermal forcing helps to set the seasonal mean distribution of  $s^*$ , but wind-driven changes in ocean evaporation set the location of the large changes in ascent and deep convection seen during monsoon onset.

Furthermore, it may be appropriate to view the convecting monsoon region as a pool of high-entropy air, with the highest amplitude changes in  $s_b$  and  $s^*$  occurring where the boundaries of this pool expand or contract with the seasonal cycle. Orography may help to organize the flow, confining the pool of high-entropy air and even

insulating it from the colder midlatitudes (Chou *et al.*, 2001; Privé and Plumb, 2007b). The degree to which this high-entropy pool is altered by the land surface thermal forcing, horizontal entropy advection in the subcloud layer, and moisture radiation feedbacks deserves further exploration in separate work.

## 6.2. Dynamical constraints on divergent flow

Even if a wind–evaporation feedback is responsible for the large increases in winds and convective activity over the Arabian Sea, other dynamical mechanisms may still be relevant to the evolution of the flow. Plumb and Hou (1992) showed that an axisymmetric circulation can intensify abruptly when the upper-tropospheric flow transitions to a state that approximately conserves absolute angular momentum in the free troposphere. Boos and Emanuel (2008b) showed that the wind-dependence of ocean evaporation can strongly reduce the critical thermal forcing needed to achieve such a nonlinear response in axisymmetric models, but that angular momentum conservation still exerts a strong constraint on the dynamics. In three dimensions, the initiation of deep-tropospheric, thermally direct flow is associated with upper-level potential vorticity (PV) that approaches zero in a region of upper-level divergence (Plumb, 2007). The time-mean PV generally remains non-zero because steady flow is not achieved in three dimensions, as the upper-level outflow of low PV air spreads westward in a ‘beta plume’ (Rhines, 1983), becomes unstable, and sheds vorticity in anticyclonic eddies (Hsu and Plumb, 2000).

The westward extension of the  $s^*$  increase that accompanies jet onset (Figure 10) is suggestive of such a beta plume, and the upper-level PV field also exhibits consistent changes during the process of jet onset. To illustrate this, we present the composite evolution of Ertel’s PV on the 350 K isentropic surface, which is typically positioned near 200 hPa in late May and early June. While Hsu and Plumb (2000) found that vorticity shedding events during peak boreal summer were most clearly evident between 360 K and 380 K, and that at 350 K the low PV outflow was not clearly separated from the low PV in the Tropics, we obtain a fairly clear signal at 350 K when examining PV anomalies relative to the date of jet onset. Furthermore, the NCEP reanalysis provides PV at 350 K directly, which is both more convenient and less prone to interpolation errors than the construction of a PV field in the range 360–380 K from pressure- or sigma-level data. Averaged from 50°E to 110°E, the onset of the Somali jet is seen to occur during a poleward shift of the 0.5 PVU contour from 20 to 30°N at 350 K (Figure 16(a)). Shortly after the onset of the jet, the zero PV contour shifts off the Equator into the Southern Hemisphere. The poleward shift of the 0.5 PVU contour in this limited zonal mean is actually due to a large PV reduction centred over the southwest edge of the Tibetan Plateau, roughly coincident with the concurrent increase in upper-tropospheric  $s^*$  (cf. Figures 16(b) and 10(b)). A strong reduction in PV is also collocated with the increase in  $s^*$  that occurs

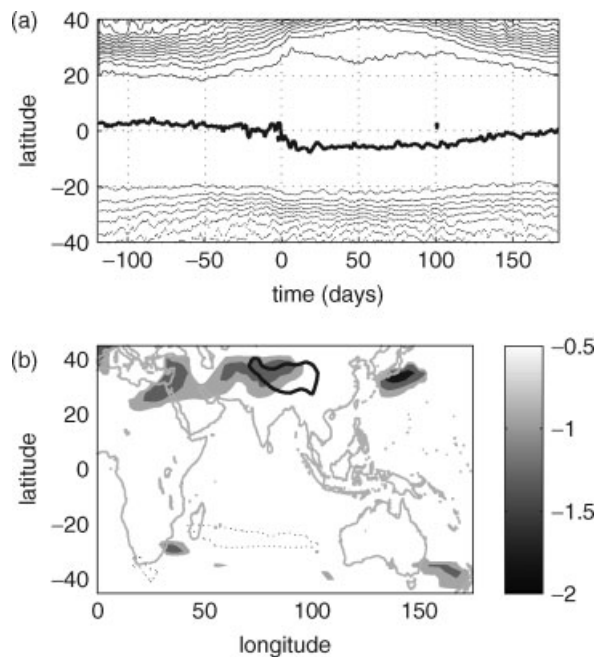


Figure 16. (a) shows the composite evolution of Ertel’s potential vorticity at 350 K, from the NCEP reanalysis, averaged between 50°E and 110°E. Time is the number of days before jet onset. The contour interval is 0.5 PVU ( $1 \text{ PVU} = 10^{-6} \text{ K m}^2 \text{ kg}^{-1} \text{ s}^{-1}$ ), with positive contours solid, negative dashed, and the zero contour denoted by the thick black line. (b) shows the change in PV over the 10 days before jet onset. Shading denotes a decrease and dotted contours an increase, and the contour interval is 0.5 PVU with the zero contour omitted.

near Japan. Both of these PV anomalies are zonally elongated, with a plume-like structure that extends westward from the peak. A time series confirms that the continental anomaly does originate over the southwestern edge of the Tibetan Plateau several days before jet onset, then extends predominantly westward across Africa as far as the eastern Atlantic Ocean over the ensuing 20 days (not shown). Such a progression is at least qualitatively consistent with the formation of an upper-tropospheric beta plume.

Hsu and Plumb (2000) found that the geopotential signal of upper-level PV anomalies in the Tibetan anticyclone during boreal summer did not extend below about 400 hPa, which is consistent with our finding that the changes in barotropic geopotential that occur during jet onset oppose the low-level baroclinic changes associated with the evolution of  $s^*$ . Examination of the vertical structure of the temperature field at 60°E confirms that the changes in  $s^*$  accompanying jet onset do extend through the full depth of the troposphere (not shown), so that the lack of any signal in the geopotential field at low levels near 30°N is not due to the absence of a signal in the  $s^*$  field at those levels.

In summary, we suggest that the formation of a beta plume and the shedding of upper-level vorticity anomalies may be involved in the poleward expansion of high free-tropospheric temperatures during monsoon onset, but that the dynamical signal of these events is confined to the upper troposphere, perhaps by the effects of surface drag. Whether vorticity shedding in three dimensions is theoretically associated with an abrupt transition similar

to that seen in axisymmetric models has not been explored; perhaps such shedding is simply a consequence, rather than a cause, of the abrupt intensification of thermally direct monsoon flow.

### 6.3. Boundary-layer momentum advection

While upper-level vorticity is relevant to the onset of deep-tropospheric divergent flow off the Equator, the evolution of low-level vorticity has been used to suggest that symmetric instability is relevant to the abrupt onset of the South Asian monsoon. Composites of the absolute vorticity,  $\eta$ , of the 850 hPa horizontal wind show that the  $\eta = 0$  contour shifts from about 3°N to 8°N over the central Arabian Sea during the 10 days preceding jet onset (Figure 11). This poleward shift in the low-level  $\eta = 0$  contour is accompanied by a large increase in ascent north of the contour and a weak increase in subsidence south of the contour, a dynamical configuration that has been used to suggest that symmetric or inertial instability is responsible for the abrupt onset of the South Asian monsoon (e.g. Krishnakumar and Lau, 1997). However, such a mechanism relies on a positive feedback between low-level moisture convergence and convective heating to continually destabilize the vorticity distribution (as detailed by Krishnakumar and Lau, 1998), otherwise the meridional circulation induced by the instability would simply relax the  $\eta = 0$  contour back toward its critically stable location on the Equator. Invoking symmetric instability to explain the abrupt onset of monsoon flow is thus equivalent to invoking conditional instability of the second kind (CISK), in which a positive feedback between low-level moisture convergence and latent heating produce a transfer of energy from a reservoir of available potential energy (APE) to the motion of the circulation. Emanuel *et al.* (1994) discussed how the moisture convergence closures on which CISK theories rely allow APE to accumulate when the precipitation is not strongly positive, then cause this APE to be released when low-level moisture convergence is strong, largely ignoring the fact that deep moist convection is a response to a local convective instability. Furthermore, symmetric instability is associated with disturbances having a high vertical wavenumber (e.g. Dunkerton, 1981), which is inconsistent with the deep-tropospheric circulations that accompany the poleward displacement of the low-level  $\eta = 0$  contour.

This is not to say that the poleward shift of the low-level  $\eta = 0$  contour is dynamically irrelevant, because it could be associated with enhanced meridional flow even in the absence of any instability. Rodwell and Hoskins (1995) showed that fluid parcels did accelerate, in a Lagrangian sense, along the trajectory of a simulated Somali jet in regions where the PV was locally anticyclonic. Also, Tomas *et al.* (1999) found that in regions of locally anticyclonic absolute vorticity in an axisymmetric boundary-layer model, the intensity of meridional flow increased nonlinearly with a specified pressure gradient forcing, even though the model was inertially stable. But their results, which are consistent

with the finding by Krishnamurti and Wong (1979) that the Somali jet satisfies a nonlinear momentum balance near the Equator, did not address the question of what sets the pressure gradient forcing. Our composites (e.g. Figure 12) show that large changes in the pressure gradient occur concurrently with jet onset and so cannot be seen as an external forcing. It is thus unclear whether nonlinear momentum advection in the boundary layer plays an important role in causing the abrupt increase in zonal wind and deep ascent over the Arabian Sea.

## 7. Summary and conclusions

Composites of the seasonal intensification of the Somali jet were compiled with the intent of characterizing and better understanding the abrupt onset of this component of the South Asian summer monsoon. A jet index was defined and used to show that the speed of low-level southwesterlies over the Arabian Sea increases faster than can be accounted for by a linear response to the insolation forcing. Cross-equatorial flow associated with the Somali jet was found to consist of a zonally focused core of southerlies near the East African highlands that increases in speed nearly linearly over about two months, and a broader region of southerly flow to the east of this core that evolves more rapidly, in concert with the off-equatorial southwesterlies. Each of these regions accounts for roughly one quarter of the global low-level, cross-equatorial mass flux.

During the onset of the jet, high-amplitude, nearly collocated increases occur in low-level southwesterlies, deep tropospheric ascent, and surface enthalpy fluxes over the Arabian Sea. The increase in ascent is roughly linearly related to the increase in the vertically integrated moist static energy source, which in turn is due mostly to an increase in ocean evaporation. This particular finding is consistent with a wind–evaporation feedback, in which surface enthalpy fluxes intensify concurrently with cross-equatorial Hadley flow (Numaguti, 1995; Boos and Emanuel, 2008a). The fact that peak free-tropospheric temperatures are located about 1000 km poleward of these large increases in ocean evaporation and ascent suggests that the wind-driven evaporation may actually cause, rather than merely correlate with, the increases in deep convection and ascent seen over the Arabian Sea. Otherwise, one would expect the maximum ascent to be positioned closer to the temperature peak, as in the dry models of Lindzen and Hou (1988) and in the moist model of Boos and Emanuel (2008a), which did not have a land surface to suppress the wind–evaporation feedback in part of the domain. The nonlinear relationship seen over land between weaker time variations in ascent and the local moist static energy source suggests that changes in either the gross moist stability or the horizontal advection of moist static energy may be important in continental regions.

A convective QE framework was judged to be at least roughly consistent with the mean summer state of the South Asian monsoon, and showed that the Tibetan

Plateau does not serve as the dominant entropy source for this circulation. However, the orographic boundaries of the plateau may serve to organize the flow of high-entropy air from the neighbouring ocean. During jet onset, the region of high subcloud entropy begins to intrude inland from the Bay of Bengal toward the base of the Tibetan Plateau. At the same time, peak tropospheric temperatures shift northwest from their position just east of the Bay of Bengal, and the region of high free-tropospheric temperatures expands poleward in a westward fashion that may be associated with the shedding of upper-level vorticity anomalies (e.g. Plumb, 2007). Barotropic geopotential changes seem to effectively confine the dynamical signal of temperature changes over land to the upper troposphere. In their study of a wind–evaporation feedback in solstitial Hadley flow, Boos and Emanuel (2008a) found a similar cancellation between barotropic and baroclinic changes away from the ascent zone because of the damping effects of surface drag.

Although this work focused almost exclusively on the mechanisms responsible for the onset of the South Asian summer monsoon, we recognize that the prediction and predictability of onset is a topic of considerable importance (e.g. Wang, 2006, and references therein). Halpern and Woiceshyn (2001) already noted that the onset of the Somali jet precedes the onset of Indian monsoon rainfall by several days; our work confirms that the onset of this jet is an important quantity to monitor for both the regional Indian monsoon and for the evolution of a large fraction of the zonal mean Hadley flow. If a wind–evaporation feedback is responsible for the abrupt nature of monsoon onset, it would be important for dynamical models used in forecasting onset to have accurate representations of surface enthalpy fluxes. Unfortunately, the mechanism of a wind–evaporation feedback would not seem to provide any considerable advance notice of monsoon onset, as winds, ocean evaporation and the large-scale circulation all intensify concurrently.

This work is only a preliminary investigation into the convectively coupled dynamics of the South Asian monsoon, and more extensive analyses using similar conserved variable approaches might provide useful information on both the mean state and seasonal evolution of this monsoon. One obvious next step is a detailed diagnosis of the evolution of all terms in the moist static energy budget, including horizontal advection and the gross moist stability. Another next step, although one that seems less straightforward to accomplish, is the development of a better understanding of the controls on moist convection and free-tropospheric temperature over land. In other words, is the approximate collocation of the  $s_b$  and  $s^*$  peaks a consequence of the validity of convective QE in this region, or merely a coincidence? If the slight inland bias in the position of the  $s^*$  peak compared to the  $s_b$  peak does not simply result from reanalysis errors, why does such a bias occur? Finally, we note the need for careful numerical simulations performed in the context of observations to more clearly understand the convectively coupled dynamics of the Somali jet and the larger monsoon.

## Acknowledgement

This research constituted part of the first author's doctoral thesis, and was supported by the National Science Foundation under grant ATM-0432090. Conversations with Alan Plumb, Richard Lindzen, and Zhiming Kuang were important in the development of this work, and we thank Martin Tingley for advice on statistical analyses. Comments by Nikki Privé and an anonymous reviewer improved this manuscript. Interpolated OLR data and NCEP reanalysis data were provided by the NOAA–CIRES Climate Diagnostics Center in Boulder, Colorado through their web site at <http://www.cdc.noaa.gov>.

## References

- Boos WR, Emanuel KA. 2008a. Wind–evaporation feedback and abrupt seasonal transitions of weak, axisymmetric Hadley circulations. *J. Atmos. Sci.* **65**: 2194–2214.
- Boos WR, Emanuel KA. 2008b. Wind–evaporation feedback and the axisymmetric transition to angular momentum conserving Hadley flow. *J. Atmos. Sci.* **65**: 3758–3778.
- Chang C-P, Wang Z, McBride J, Liu C-H. 2005. Annual cycle of Southeast Asia–Maritime Continent rainfall and the asymmetric monsoon transition. *J. Climate* **18**: 287–301.
- Chou C, Neelin JD, Su H. 2001. Ocean–atmosphere–land feedbacks in an idealized monsoon. *Q. J. R. Meteorol. Soc.* **127**: 1869–1892.
- Dima IM, Wallace JM. 2003. On the seasonality of the Hadley cell. *J. Atmos. Sci.* **60**: 1522–1527.
- Dunkerton TJ. 1981. On the inertial stability of the Equatorial middle atmosphere. *J. Atmos. Sci.* **38**: 2354–2364.
- Durre I, Russell SV, Wuertz DB. 2006. Overview of the Integrated Global Radiosonde Archive. *J. Climate* **19**: 53–68.
- Emanuel KA. 1987. Air–sea interaction model of intraseasonal oscillations in the Tropics. *J. Atmos. Sci.* **44**: 2324–2340.
- Emanuel KA. 1995. On thermally direct circulations in moist atmospheres. *J. Atmos. Sci.* **52**: 1529–1536.
- Emanuel KA, Neelin JD, Bretherton CS. 1994. On large-scale circulations in convecting atmospheres. *Q. J. R. Meteorol. Soc.* **120**: 1111–1143.
- Findlater J. 1969. A major low-level air current near the Indian Ocean during the northern summer. *Q. J. R. Meteorol. Soc.* **95**: 362–380.
- Findlater J. 1971. *Mean monthly air flow at low levels over the western Indian Ocean*. Geophys. Mem. 53; HMSO: London.
- Findlater J. 1972. Aerial explorations of the low-level cross-equatorial current over eastern Africa. *Q. J. R. Meteorol. Soc.* **98**: 274–289.
- Flohn H. 1974. Contribution to a comparative meteorology of mountain areas. *Arctic and Alpine Environments*. Ives JD, Barry RG. (eds.) Methuen: London, pp 55–71.
- Gill AE. 1980. Some simple solutions for heat-induced tropical circulation. *Q. J. R. Meteorol. Soc.* **106**: 447–462.
- Goswami BN, Sengupta D. 2003. A note on the deficiency of NCEP/NCAR reanalysis surface winds over the equatorial Indian Ocean. *J. Geophys. Res.* **108**: 3124.
- Hahn DG, Manabe S. 1975. The role of mountains in the South Asian monsoon circulation. *J. Atmos. Sci.* **32**: 1515–1541.
- Halpern D, Woiceshyn PM. 1999. Onset of the Somali Jet in the Arabian Sea during June 1997. *J. Geophys. Res.* **104**: 18 041–18 046.
- Halpern D, Woiceshyn PM. 2001. Somali Jet in the Arabian Sea, El Niño, and India Rainfall. *J. Climate* **14**: 434–441.
- Halpern D, Freilich MH, Weller RA. 1999. ECMWF and ERS-1 surface winds over the Arabian Sea during July 1995. *J. Phys. Oceanogr.* **29**: 1619–1623.
- Hart JE, Rao G, Van De Boogaard H, Young JA, Findlater J. 1978. Aerial observations of the East African low-level jet stream. *Mon. Weather Rev.* **106**: 1714–1724.
- Held IM, Hou AY. 1980. Nonlinear axially symmetric circulations in a nearly inviscid atmosphere. *J. Atmos. Sci.* **37**: 515–533.
- Hsu CJ, Plumb RA. 2000. Non-axisymmetric thermally driven circulations and upper-tropospheric monsoon dynamics. *J. Atmos. Sci.* **57**: 1255–1276.
- Kalnay E, Kanamitsu M, Kirtler R, Collins W, Deaven D, Gandin L, Iredell M, Saha S, White G, Woollen J, Zhu Y, Chelliah M, Ebisuzaki W, Higgins W, Janowiak J, Mo KC, Ropelewski C,

- Wang J, Leetma A, Reynolds R, Jenne R, Joseph D. 1996. The NCEP/NCAR 40-year reanalysis project. *Bull. Am. Meteorol. Soc.* **77**: 437–472.
- Krishnakumar V, Lau K-M. 1997. Symmetric instability of monsoon flows. *Tellus A* **49**: 228–245.
- Krishnakumar V, Lau K-M. 1998. Possible role of symmetric instability in the onset and abrupt transition of the Asian Monsoon. *J. Meteorol. Soc. Jpn.* **76**: 363–383.
- Krishnamurti TN. 1985. Summer Monsoon Experiment – A review. *Mon. Weather Rev.* **113**: 1590–1626.
- Krishnamurti TN, Bhalme HN. 1976. Oscillations of a monsoon system. Part I. Observational aspects. *J. Atmos. Sci.* **33**: 1937–1954.
- Krishnamurti TN, Wong V. 1979. A planetary boundary-layer model for the Somali Jet. *J. Atmos. Sci.* **36**: 1895–1907.
- Krishnamurti TN, Molinari J, Pan HL. 1976. Numerical simulation of the Somali Jet. *J. Atmos. Sci.* **33**: 2350–2362.
- Krishnamurti TN, Ardanuy P, Ramanathan Y, Pasch R. 1981. On the onset vortex of the summer monsoon. *Mon. Weather Rev.* **109**: 344–363.
- Krishnamurti TN, Wong V, Pan H-L, Pasch R, Molinari J, Ardanuy P. 1983. A three-dimensional planetary boundary-layer model for the Somali Jet. *J. Atmos. Sci.* **40**: 894–908.
- Li C, Yanai M. 1996. The onset and interannual variability of the Asian summer monsoon in relation to land–sea thermal contrast. *J. Climate* **9**: 358–375.
- Lindzen RS, Hou AY. 1988. Hadley circulation for zonally averaged heating centered off the Equator. *J. Atmos. Sci.* **45**: 2416–2427.
- Livezey RE, Chen WY. 1983. Statistical field significance and its determination by Monte Carlo Techniques. *Mon. Weather Rev.* **111**: 46–59.
- Molnar P, Emanuel KA. 1999. Temperature profiles in radiative-convective equilibrium above surfaces at different heights. *J. Geophys. Res.* **104**: 24 265–24 272. DOI: 10.1029/1999JD900485.
- Neelin JD, Held IM. 1987. Modeling tropical convergence based on the moist static energy budget. *Mon. Weather Rev.* **115**: 3–12.
- Neelin JD, Held IM, Cook KH. 1987. Evaporation–wind feedback and low-frequency variability in the tropical atmosphere. *J. Atmos. Sci.* **44**: 2341–2348.
- Neelin JD, Zeng N. 2000. A quasi-equilibrium tropical circulation model: Formulation. *J. Atmos. Sci.* **57**: 1741–1766.
- Numaguti A. 1995. Dynamics and energy balance of the Hadley circulation and the tropical precipitation zones. Part II: Sensitivity to meridional SST distribution. *J. Atmos. Sci.* **52**: 1128–1141.
- Plumb RA. 2007. Dynamical constraints on monsoon circulations. *The Global Circulation of the Atmosphere*. Schneider T, Sobel AH. (eds.) Princeton University Press: Princeton, New Jersey, pp 252–266.
- Plumb RA, Hou AY. 1992. The response of a zonally symmetric atmosphere to subtropical thermal forcing: Threshold behavior. *J. Atmos. Sci.* **49**: 1790–1799.
- Privé NC, Plumb RA. 2007a. Monsoon dynamics with interactive forcing. Part I: Axisymmetric studies. *J. Atmos. Sci.* **64**: 1417–1430.
- Privé NC, Plumb RA. 2007b. Monsoon dynamics with interactive forcing. Part II: Impact of eddies and asymmetric geometries. *J. Atmos. Sci.* **64**: 1431–1442.
- Raymond DJ. 1995. Regulation of moist convection over the West Pacific warm pool. *J. Atmos. Sci.* **52**: 3945–3959.
- Rhines P. 1983. Lectures on geophysical fluid dynamics. *Lec. Appl. Math.* **20**: 1–58.
- Rodwell MJ, Hoskins BJ. 1995. A model of the Asian summer monsoon. Part II: Cross-equatorial flow and PV behavior. *J. Atmos. Sci.* **52**: 1341–1356.
- Rodwell MJ, Hoskins BJ. 1996. Monsoons and the dynamics of deserts. *Q. J. R. Meteorol. Soc.* **122**: 1385–1404.
- Rossov WB, Zhang YC. 1995. Calculation of surface and top of atmosphere radiative fluxes from physical quantities based on ISCCP data sets. 2: Validation and first results. *J. Geophys. Res.* **100**(D1): 1167–1197.
- Tomas RA, Holton JR, Webster PJ. 1999. The influence of cross-equatorial pressure gradients on the location of near-equatorial convection. *Q. J. R. Meteorol. Soc.* **125**: 1107–1127.
- Wang B. 2006. *The Asian monsoon*. Springer-Praxis Publishing: Berlin.
- Webster PJ, Magana VO, Palmer TN, Shukla J, Tomas RA, Yanai M, Yasunari T. 1998. Monsoons: Processes, predictability, and the prospects for prediction. *J. Geophys. Res.* **103**: 14 451–14 510.
- Weickmann KM, Chervin RM. 1988. The observed and simulated atmospheric seasonal cycle. Part I: Global wind field modes. *J. Climate* **1**: 265–289.
- Weller RA, Baumgartner MF, Josey SA, Fischer AS, Kindle JC. 1998. Atmospheric forcing in the Arabian Sea during 1994–1995: Observations and comparisons with climatology and models. *Deep-Sea Res.* **45**: 1961–1999.
- Xie S-P, Saiki N. 1999. Abrupt onset and slow seasonal evolution of summer monsoon in an idealized GCM simulation. *J. Meteorol. Soc. Jpn.* **77**: 949–968.
- Yu L, Weller RA. 2007. Objectively analyzed air–sea heat fluxes for the global ice-free oceans (1981–2005). *Bull. Am. Meteorol. Soc.* **88**: 527–539.
- Yu L, Weller RA, Sun B. 2004. Improving latent and sensible heat flux estimates for the Atlantic Ocean (1988–99) by a synthesis approach. *J. Climate* **17**: 373–393.
- Yu, L, Jin X, Weller RA. 2007. Annual, seasonal, and interannual variability of air–sea heat fluxes in the Indian Ocean. *J. Climate* **20**: 3190–3209.